SPECTROSCOPY OF MARS ATMOSPHERE FROM ORBITING AND GROUND-BASED OBSERVATORIES: RECENT RESULTS AND IMPLICATIONS FOR EVOLUTION. V. A. Krasnopolsky, Catholic University of America, Department of Physics, 200 Hannan Hall, Washington, D.C. 20064 (vkrasn@verizonmail.com).

Introduction: The basic data on the chemical composition of Mars' atmosphere were obtained by the Viking mass spectrometers a quarter of century ago. Spacecraft missions to Mars in the last decade have not been aimed to this field, and the current progress is related to high-resolution spectroscopy from orbiting and ground-based observatories.

HDO: Deuterated water was detected [1] using CFHT/FTS with resolving power $\nu/\delta\nu = 9\times10^4$ (Fig. 1). Very low humidity (0.5 pr. mm) above Mauna Kea and a significant (by a factor of 6) enrichment of water in D on Mars facilitated the detection.

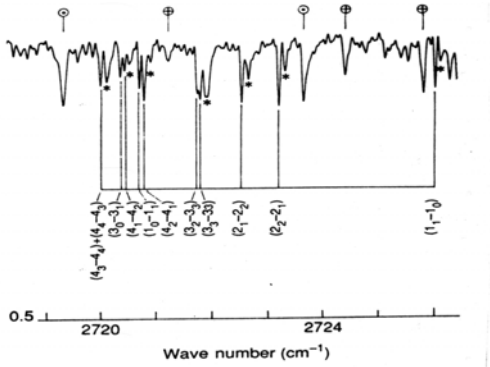

Fig.1. HDO lines in the CFHT/FTS spectrum [1]. Telluric HDO (*), CH_4 (+), and solar (·) lines are also seen.

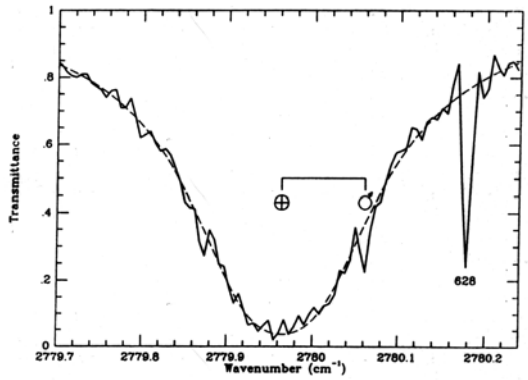

Fig. 2. One of ten HDO lines in the KPNO/FTS spectrum [2]. Telluric line is much stronger and broader than the Martian line. Dashed curve is a model fit to the telluric line, 628 is the $CO^{18}O$ line.

Ten HDO lines in the KPNO/FTS spectrum [2] were also used to measure the D/H ratio in water on Mars (Fig. 2). Despite the better spectral resolution ($\nu/\delta\nu = 2.7\times10^5$), the HDO lines were less prominent because of the much higher humidity (14 pr. mm) above Kitt Peak. Both observations agree and result in D/H = 5.5 ± 1 times the terrestrial value in the Martian water. The KAO observation of HDO [3] is still under revision.

Atomic Deuterium: The D Lyman-α line at 1215.34 Å is shifted from the H line by 0.33 Å and very much weaker than the H line. The Martian lines are Doppler-shifted by 0.06 Å maximum relative to the telluric lines. All four lines were detected and resolved (Fig. 3) in the HST/GHRS observation [4]. The instrument resolving power was 1.6×10^4. The observed D-line intensity of 23 ± 6 R at solar minimum corresponds to [D] = 450 ± 120 cm^{-3} at 250 km.

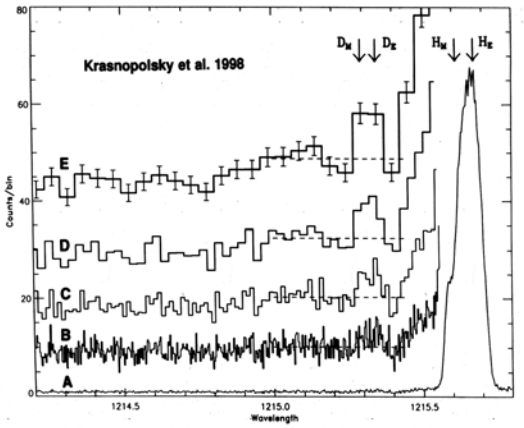

Fig. 3. Telluric and Martian (subscripts E and M, respectively) Lyman-α lines of H and D in the HST/GHRS spectrum [4] at five levels of binning.

Molecular Hydrogen: Vibrational and rotational transitions are strongly forbidden in H_2. Despite the low dissociation energy of 4.48 eV, dissociation to the ground-state H atoms is parity-forbidden, and H_2 absorbs photons only below 1108 Å where the solar radiation is weak. Therefore, detection of H_2 presents a difficult problem. Fortunately, three absorption lines of H_2 coincide with the strong solar Lyman β, γ, and C II lines and originate a few comparatively strong emission lines. These lines were observable (Fig. 4) in the FUSE spectrum of Mars [5]. The observation resulted in a column H_2 abundance of $(1.71 \pm 0.13)\times10^{13}$ cm^{-2} above 140 km. The FUSE spectrum of Mars [6] covered a range of 904 to 1186 Å with spectral resolution of 0.2 Å. The spectrum is of high quality and provides a detection limit of ≈0.1 R. Many Martian lines and

ion species N^+, C^+, and Ar^+ have been observed for the first time in that spectrum. For example, two Ar^+ and eight H lines of the Lyman series are among other lines in Fig. 5.

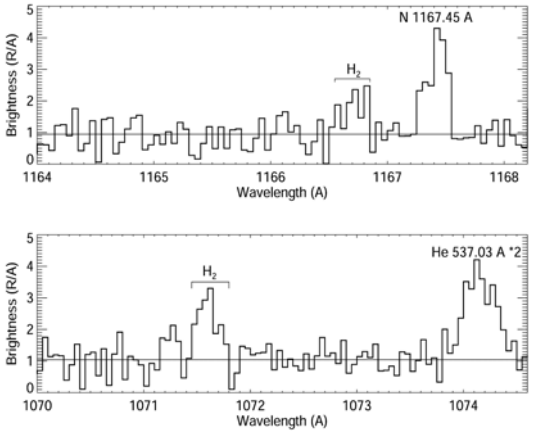

Fig. 4. Fragments of the FUSE spectrum [5] near the H_2 lines at 1166.76 and 1071.62 Å.

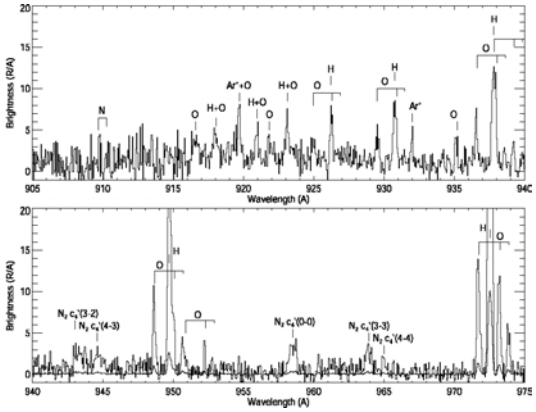

Fig. 5. A part of the FUSE spectrum [6].

Interpretation of the Observed HDO, D, and H_2:

Detailed photochemical modeling of Mars' upper atmosphere and ionosphere [7] to fit the observed D and H_2 abundances results in the HD and H_2 mixing ratios of 11± 4 ppb and 15 ± 5 ppm, respectively. Then

$$R = \frac{HD/H_2}{HDO/H_2O} = 0.4.$$

This agrees with the fractionation of D in chemical reactions (R ≈ 1.6 [8]), photolysis of H_2O (R ≈ 0.4 [9], and the HDO depletion above the condensation level (R ≈ 0.7 [10, 11])). Finally, R = 1.6×0.4×0.7 ≈ 0.4, and the controversial problem of deuterium fractionation in Mars' atmosphere looks solved. The observed HDO, D, and H_2 require the escape fractionation factor

$$f = \frac{\phi_D/\phi_H}{D/H} = 0.105$$

averaged over the solar cycle.

Implications for Evolution of Water: Combining this fractionation factor with the water abundance in the polar caps (a global-mean layer of ≈14 m deep [12-14]) and the D/H = 1.9 [15] at the end of the intense impact erosion of the atmosphere 3.8 Ga ago, this results in a loss of an ocean of water of 30 m deep for this period.

Hydrodynamic escape of H_2 released in the reaction Fe + H_2O → FeO + H_2 could be effective for 0.1-0.3 Ga after Mars' formation. Using a fractionation factor of 0.8 for this escape [16] and a standard assumption of the terrestrial value for the initial D/H on Mars, the total loss of water by hydrodynamic escape was 1.2 km. Therefore Mars could initially be even more rich in water than Earth.

Helium: Helium was detected on Mars using the EUVE/LW spectrometer [17] that had a capability to detect the He 584 Å line against the strong geocoronal emission of this line. The observed line intensity of 57 ± 15 R corresponds to the He mixing ratio of 4 ± 2 ppm [18]. Helium is lost from Mars mostly by electron impact ionization above the ionopause and sweeping out of the ions by the solar wind. The total loss is equal to 7×10^{23} s^{-1} and agrees with the Phobos measurements [19]. A source of He on the terrestrial planets is the radioactive decay in the uranium and thorium chains with subsequent outgassing. It is similar to the outgassing of ^{40}Ar formed by the decay of potassium. A coupled model for the outgassing of He and ^{40}Ar showed that (1) outgassing from Mars is weaker than that from Earth by an order of magnitude, (2) outgassing of He from Mars covers a third of its loss. An additional source of He is required, and that should be a capture of the solar-wind α-particles with an efficiency of ≈0.3. This is the first and probably the only case when a capture of the solar wind is critical to a

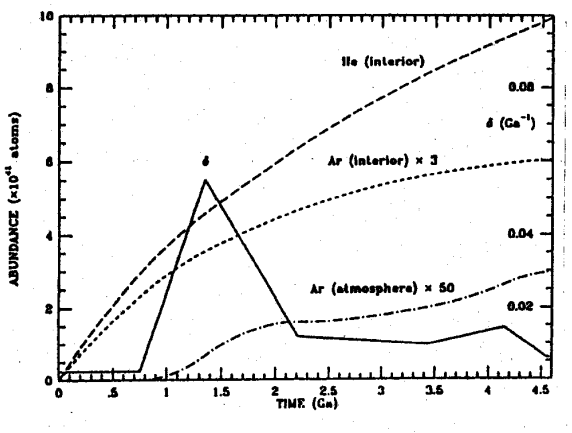

Fig. 6. Model [18] for evolution of ^{4}He and ^{40}Ar in Mars interior and atmosphere for outgassing coefficient δ proportional to Mars volcanism rate from [20].

balance of atmospheric species. Later calculations of the solar wind capture efficiency by Mars [21] confirmed our conclusion and also gave the value of 0.3 for α-particles.

Ozone and O_2 1.27 μm Dayglow: Ozone is a tracer of Mars photochemistry, and a latitudinal-versus-season mapping of O_3, similar to that done for H_2O by the Viking/MAWD [22] and MGS/TES [23], is the objective of ozone observations. Three tools are currently used. Infrared heterodyne spectroscopy at 9.6 μm [24] gave the first data on the O_3 distribution at low and middle latitudes (Fig. 6). The instrument resolving power was 10^6 in the published observations. Another tool is the HST/FOS UV spectroscopy near Mars' limb [25, 26] (Fig. 7).

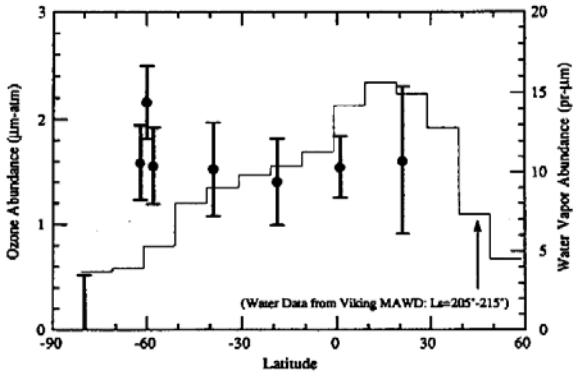

Fig. 6. Latitudinal distribution of ozone at L_S = 208° [24].

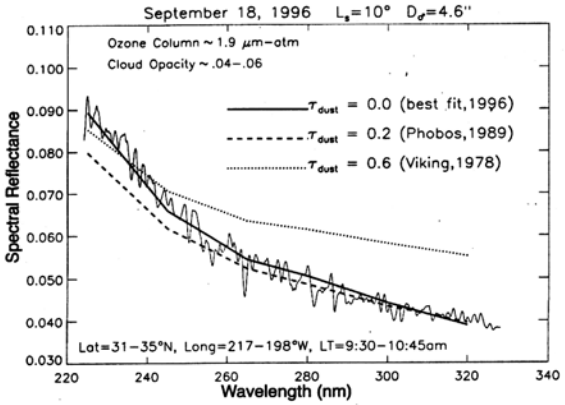

Fig. 7. Three-parameter fitting to the observed HST/FOS spectrum [26] near Mars' limb. The parameters are ozone column and cloud and dust opacities.

Ozone above 20 km is the most sensitive to seasonal variations of photochemistry at low and middle latitudes [27]. It was suggested in [28] to observe the O_2 1.27 μm dayglow using IRTF/CSHELL to map high-altitude ozone. This dayglow is excited by photolysis of O_3 and quenched by CO_2 below 15-20 km. Therefore it is the best tracer of Mars' photochemistry. The IRTF/CSHELL resolving power is 4×10^4, that is, 7.5 km/s, and the observations are feasible for the geocentric velocity ≥ 10 km/s. The dayglow spectrum observed at L_S = 112° [29] is shown in Fig. 8. The retrieved dayglow intensities are corrected for airmass, surface reflectivity, and the instrument point spread function. (All these corrections are of a factor of ≈1.5 and cannot be ignored.) Latitudinal dependences of the dayglow intensity for three seasons [30] are shown in Fig. 9. The dayglow maps have a spatial resolution of 0.1-0.2 Mars radii. Analysis of the dayglow observation along one instrument slit was recently reported in [31].

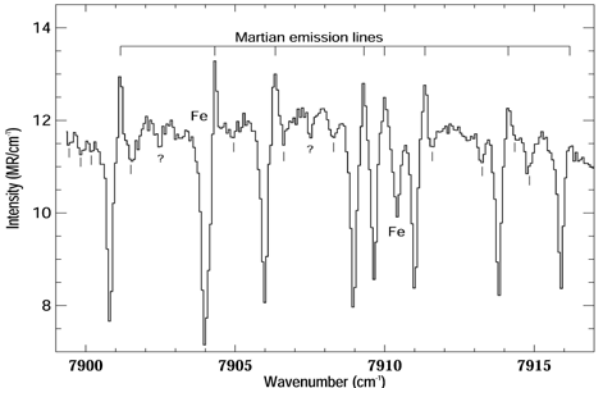

Fig. 8. One of 550 spectra of Mars observed with IRTF/CSHELL at L_S =112° [29]. The main features are the telluric absorption and Martian Doppler-shifted O_2 emission lines and two solar Fe lines.

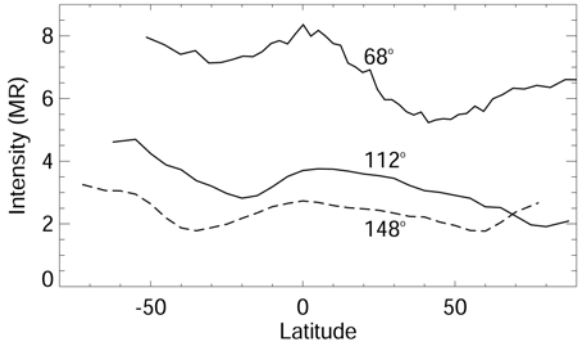

Fig. 9. Latitudinal dependences of the O_2 1.27 μm dayglow at three seasons [30].

CO Mixing Ratio: Low resolution spectroscopy from the Phobos orbiter [32] revealed a significant (by a factor of 5-8) decrease in the CO mixing ratio above the great Martian volcanoes. This decrease contradicts to gas-phase chemistry, which predicts a constant CO mixing ratio over Mars' globe and up to ≈60 km. Attempts to check this result by using ground-based observations were made in [33, 34] using the CO lines at

1.3 mm and 2.3 μm, respectively. However, their fields of view were large, 1 and 0.5 Mars radii, respectively. No significant variations have been observed. A CO line shape at 1.3 mm [35] also favors a CO mixing ratio, which is constant with height.

The CO mixing ratio on Mars was mapped at L_S =112° [36] by observing both CO and CO_2 lines at 1.57 μm (Fig. 10) using IRTF/CSHELL. The measured CO mixing ratio does not vary from place to place, with local time and elevation (in the range of -6 to 3 km) while the variation with latitude is substantial (Fig. 11). It is explained by the intense condensation of CO_2 at the South (winter) polar cap and the low meridional circulation in the southern winter [37]. An alternative explanation is the photochemical accumulation of CO due to freezing out of H_2O. However, it is compensated by the low insolation in winter polar regions (polar night) and much smaller than the observed effect. The increase in the CO mixing ratio to the South and its extent to low latitudes is determined by atmospheric dynamics and should be simulated by GCMs.

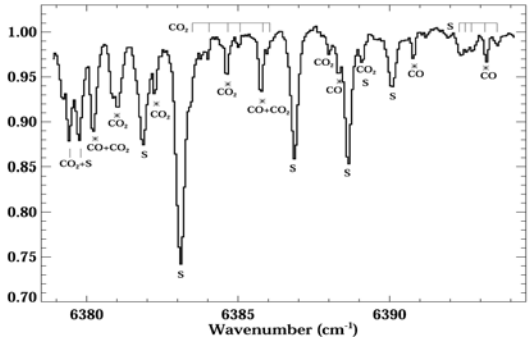

Fig. 10. One of 520 IRTF/CSHELL spectra at 1.57 μm [36]. The spectrum consists of the CO, CO_2, and solar (S) lines.

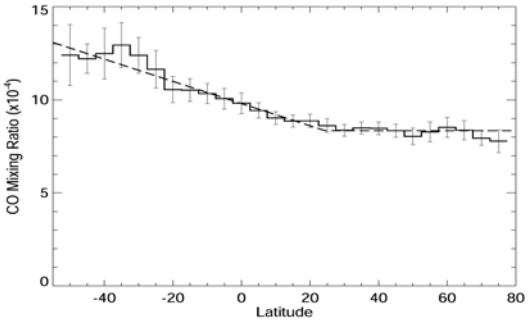

Fig. 11. Latitudinal dependence of the CO mixing ratio at L_S = 112° [36].

Upper Limits: The most restrictive upper limit was obtained recently for H_2O_2 using TEXES at 8 μm. The instrument resolving power was 7×10^4, and the limit is 4 ppb [38], that is, below the model predictions by an order of magnitude. Upper limits of 3 ppb to HCl and H_2CO were extracted from the KPNO/FTS spectrum at 3.7 μm [2]. The limit to HCl shows that chlorine chemistry is negligible on Mars.

Here I do not consider very fruitful and extensive MGS/TES observations of temperature profiles, H_2O, dust and ice aerosol, and ground-based observations of water vapor, H_2O and CO_2 ice, and dust, and microwave observations.

Acknowledgment: This work was supported by NASA Mars Data Analysis Program (grant NAG5-10575).

References: [1] Owen T. et al. (1988) *Science 240,* 1767-1771. [2] Krasnopolsky V. A. et al. (1997) *JGR 102,* 6525-6534. [3] Bjoraker G. L. et al. (1989) *BAAS 21,* 991. [4] Krasnopolsky V. A. et al. (1998) *Science 280,* 1576-1580. [5] Krasnopolsky V. A. and Feldman P. D. (2001) *Science 294,* 1914-1917. [6] Krasnopolsky V. A. and Feldman P. D. (2002) *Icarus 160,* 86-94. [7] Krasnopolsky V. A. (2002) *JGR 107,* E12, 10.1029/2001JE001809. [8] Yung Y. L. et al. (1988) *Icarus 76,* 146-159. [9] Cheng B. M. et al. (1999) *GRL 26,* 3657-3660. [10] Fouchet T. and Lellouch E. (2000) *Icarus 144,* 114-123. [11] Krasnopolsky V. A. (2000) *Icarus 148,* 597-602. [12] Jakosky B. M. (1990) *JGR 95,* 1475-1480. [13] Smith D. E. et al. (1999) *Science 284,* 1495-1503. [14] Head J. W. (2001) *JGR 106,* 10075-10080. [15] Leshin L. A. (2000) *GRL 27,* 2017-2020. [16] Zahnle K. et al. (1990) *Icarus 84,* 502-527. [17] Krasnopolsky V. A. et al. (1994) *Icarus 109,* 337-351. [18] Krasnopolsky V. A. and Gladstone G. R. (1996) *JGR 101,* 15765-15772. [19] Barabash S. et al. (1995) *JGR 100,* 21307-213016. [20] Greeley R. (1987) *Science 236,* 1653-1654. [21] Brecht S. H. (1997) *JGR 102,* 11287-11294. [22] Jakosky B. M. and Farmer C. B. (1982) *JGR 87,* 2999-3019. [23] Smith M. D. (2002) *JGR 107,* E11, 10.1029/ 2001JE001522. [24] Espenak F. et al. (1991) *Icarus 92,* 252-262. [25] Clancy R. T. et al. (1996) *JGR 101,* 12777-12783. [26] Clancy R. T. et al. (1999) *Icarus 138,* 49-63. [27] Clancy R. T. and Nair H. (1996) *JGR 101,* 12785-12790. [28] Krasnopolsky V. A. (1997) *JGR 102,* 13313-13320. [29] Krasnopolsky V. A. and Bjoraker G. L. (2000) *JGR 105,* 20179-20188. [30] Krasnopolsky V. A. (2003) *Icarus* (submitted). [31] Novak R. et al. (2002) *Icarus 158,* 14-23. [32] Rosenqvist J. et al. (1992) *Icarus 98,* 254-270. [33] Lellouch E. et al. (1991) *PSS 39,* 219-224. [34] Billebaud F. et al. (1998) *AA 333,* 1092-1099. [35] Encrenaz T. et al. (1991) *Ann. Geo. 9,* 797-803. [36] Krasnopolsky V. A. (2003) *JGR 108,* E2, 10.1029/2002JE001926. [37] Haberle R. M. et al. (1993) *JGR 98,* 3093-3123. [38] Encrenaz T. et al. (2002) *AA 396,* 1037-1044.